

Exceptionally Enhanced Electrode Activity of (Pr,Ce)O_{2-δ}-Based Cathodes for Thin-Film Solid Oxide Fuel Cells

Han Gil Seo, Yoonseok Choi, and WooChul Jung*

It is shown that an electrochemically-driven oxide overcoating substantially improves the performance of metal electrodes in high-temperature electrochemical applications. As a case study, Pt thin films are overcoated with (Pr,Ce)O_{2-δ} (PCO) by means of a cathodic electrochemical deposition process that produces nanostructured oxide layers with a high specific surface area and uniform metal coverage and then the coated films are examined as an O₂-electrode for thin-film-based solid oxide fuel cells. The combination of excellent conductivity, reactivity, and durability of PCO dramatically improves the oxygen reduction reaction rate while maintaining the nanoscale architecture of PCO layers and thus the performance of the PCO-coated Pt thin-film electrodes at high temperatures. As a result, with an oxide coating step lasting only 5 min, the electrode resistance is successfully reduced by more than 1000 times at 500 °C in air. These observations provide a new direction for the design of high-performance electrodes for high-temperature electrochemical cells.

Solid oxide fuel cells (SOFCs) are environmentally friendly devices that convert the chemical energy of various fuels into electricity with high efficiency, overcoming the theoretical combustion limits. However, the high material and system cost and insufficient device lifetimes caused by the high temperatures (>800 °C) required for operation are great challenges hindering the success of SOFC technology.^[1–3] Recently, attempts to lower the operating temperatures (<600 °C) of these devices by introducing thin-film processes have attracted a great deal of attention, with the resulting products known as thin-film-based SOFCs (TF-SOFCs).^[4–6] The use of a solid membrane with a thickness of several hundred nanometers or less can greatly reduce the ohmic resistance of the solid electrolyte, even at low temperatures.^[7,8] Nonetheless, the electrochemical resistance of a cathode increases rapidly at a low temperature due to the high activation energy of the oxygen reduction reaction (ORR), which remains the greatest obstacle preventing the implementation of high-performance TF-SOFCs.^[9,10]


For this reason, platinum (Pt) thin-film electrodes are commonly used in TF-SOFCs due to the excellent electrical

conductivity of Pt and its good catalytic activity toward ORR.^[11,12] Furthermore, Pt is readily applicable to thin-film processes compared to the metal oxides that are often used as electrode materials but require a high calcination temperature. Despite these advantages, however, there are two critical issues to consider when using Pt films for TF-SOFCs. The first is that the electrochemical reactions at a Pt electrode can only occur at very limited sites, known as triple-phase boundaries (3PB), where the Pt, electrolyte, and gas all come into contact.^[12] The second issue is the inherently poor thermal stability of Pt thin films, which leads to severe losses of the electrode activity at elevated operating temperatures.^[13,14] Thus, making Pt-based electrodes more robust and reactive has remained a tremendous challenge.

Here, we address these issues by overcoating Pt electrodes with oxides having appropriate functionalities. (Pr,Ce)O_{2-δ} (PCO) was chosen as the coating material owing to its favorable catalytic activity and good sintering resistance. More importantly, unlike other forms of rare-earth-doped ceria, which only exhibits oxygen-ion conductivity, Pr doping forms an impurity band that acts as an electron conduction channel. Therefore, PCO can have both high ionic and electronic conductivity in high-temperature oxidizing atmospheres.^[15–17] The mixed conducting characteristics of PCO likely not only facilitate electron and ion transfer processes but also remarkably improve the electrode activity, as ORR sites can be extended from the 3PB to the entire oxide surface (double-phase boundary, 2PB). To the best of our knowledge, however, no composite electrode composed of PCO and metal has been used for TF-SOFCs.

In this study, we fabricated model symmetric electrochemical cells with Pt patterned electrodes on both sides of a yttria-stabilized ZrO₂ (YSZ) electrolyte substrate and observed the changes in the electrode activity and stability depending on the presence of the PCO overcoats at below 600 °C, at which temperatures TF-SOFCs operate. Nanostructured PCO layers were coated onto Pt surfaces via a simple, cost-effective, and scalable coating method known as cathodic electrochemical deposition (CELD). The electrode activity of the PCO-coated films was then investigated by AC impedance spectroscopy (ACIS). We found that the PCO overcoats significantly improve the ORR activity by more than 1000 times with decent thermal stability. In addition, based on the observed excellent electrode features of PCO, we even succeeded in designing a nanostructured, 1-μm-thick PCO thin-film cathode without any Pt and

H. G. Seo, Y. Choi, Prof. W. Jung
Department of Materials Science and Engineering
Korea Advanced Institute of Science and Technology
291 Daehak-ro, Yuseong-gu, Daejeon 34141, Republic of Korea
E-mail: wjung@kaist.ac.kr

 The ORCID identification number(s) for the author(s) of this article can be found under <https://doi.org/10.1002/aenm.201703647>.

DOI: 10.1002/aenm.201703647

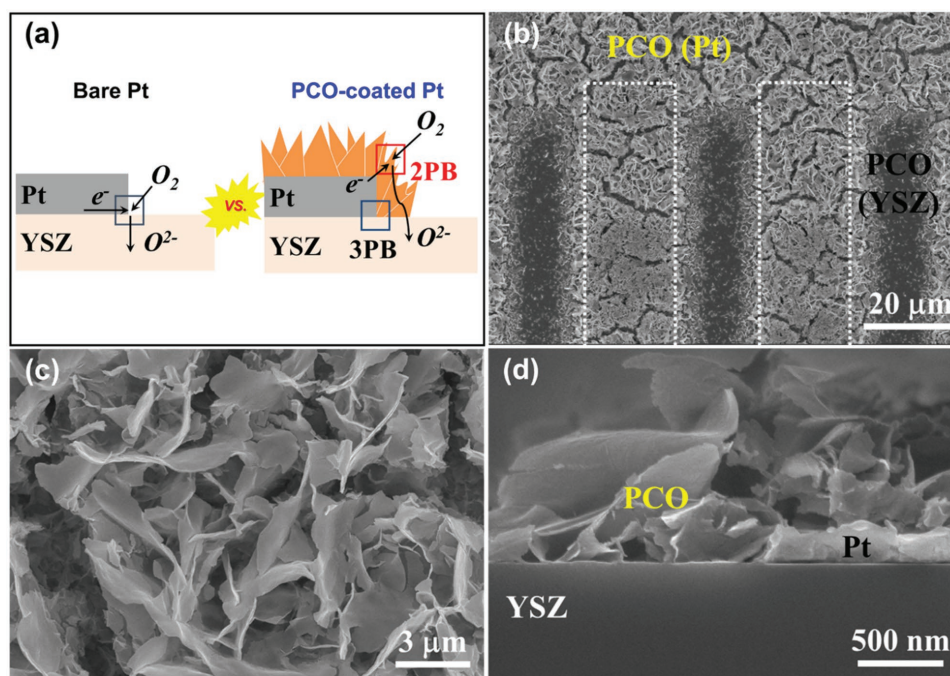


Figure 1. a) Schematic comparison of oxygen reduction reaction (ORR) sites between bare and $(\text{Pr,Ce})\text{O}_{2-\delta}$ (PCO)-coated Pt electrodes, b) SEM images of a typical $20\ \mu\text{m}$ patterned PCO-coated Pt electrode and c) a magnified image near the edge of Pt, and d) cross-sectional image of a PCO-coated Pt electrode. Cathodic electrochemical deposition (CELD) was conducted at $-0.8\ \text{V}$ versus saturated calomel electrode (SCE) for a deposition time of 300 s.

achieving an electrode resistance level of $0.6\ \Omega\ \text{cm}^2$ at $600\ ^\circ\text{C}$ in air.

Figure 1a presents schematic images showing how ORR sites vary in bare and PCO-coated Pt electrodes. In contrast to bare Pt, PCO-coated Pt has a significant number of 2PB reaction sites between PCO and O_2 , in addition to 3PB sites, because PCO conducts both electrons and oxygen ions sufficiently. To avoid greater morphological complexity associated with conventional cermet structures and to analyze the effects of the PCO overcoats accurately, we fabricated model Pt strip electrodes with well-defined interfaces. Here, the 3PB site density was controlled by varying the width of each Pt strip with a thickness of $\approx 200\ \text{nm}$. Subsequently, nanostructured PCO layers were overcoated on the patterned Pt electrodes via CELD (Figure S1, Supporting Information). Scanning electron microscopy (SEM) images of a typical $20\ \mu\text{m}$ patterned PCO-coated Pt films on a YSZ substrate are shown in Figure 1b–d. As the CELD deposition time increases, the thickness of the deposited PCO film also increases (Figure S2, Supporting Information). To obtain a sufficient specific surface area and prevent detachment of the coating film, we utilized an applied potential of $-0.8\ \text{V}$ versus a reference electrode (saturated calomel electrode, SCE) and a deposition time of 300 s (thickness of $1.8\ \mu\text{m}$) for further electrochemical analyses. The deposited PCO films exhibit both microscale cracks of $0.9\text{--}2.4\ \mu\text{m}$ and nanoscale cracks, both stemming from the volume change in the initial deposits of a hydrated cerium oxy-hydroxide to CeO_2 or partial sintering of the ceria.^[18,19] These multiscale pores allow oxygen molecules to be delivered readily to the PCO surface. It is noteworthy that unlike conventional electroplating, CELD contains a chemical precipitation process, meaning that PCO can be partially coated onto the insulating YSZ surface. Accordingly, the resulting

PCO|YSZ and PCO|Pt contacts facilitate the transfer of oxygen ions and electrons, respectively. As discussed below, these features help to activate the 2PB reaction sites (PCO| O_2 interfaces). A more detailed description of the CELD process of ceria can be found in the literature.^[11,20]

Table 1 summarizes the chemical composition of the deposited PCO films for the solution concentration used in the CELD process, as analyzed by X-ray fluorescence (XRF) and inductively coupled plasma mass spectroscopy (ICP-MS). The Pr concentration in the deposited PCO films exhibits a slightly higher value than that of the CELD bath, which may be related to the lower solubility of $\text{Pr}(\text{OH})_3$,^[21] compared to that of $\text{Ce}(\text{OH})_3$.^[22] In this study, the target composition of PCO films was determined to be $\text{Pr}_{0.21}\text{Ce}_{0.79}\text{O}_{2-\delta}$ to maximize both the ionic and electronic conductivity values at $p\text{O}_2$ levels from 10^{-4} to 10^{-1} atm and temperatures ranging from 500 to $650\ ^\circ\text{C}$.^[15,23] Indeed, a Pr content of 21% is sufficient to form a continuous Pr impurity band within the bandgap of CeO_2 , but it is not enough to induce a significant association between oxygen vacancies, which reduces oxygen-ion conductivity. Thus, electrons can readily transport between adjacent Pr ions owing to the large overlap of Pr orbitals in the ceria lattice. A related schematic

Table 1. XRF and ICP-MS composition analysis results of cathodic electrochemical deposition (CELD) $(\text{Pr,Ce})\text{O}_{2-\delta}$ (PCO) films deposited at an applied potential of $-0.8\ \text{V}$ versus saturated calomel electrode (SCE) for a deposition time of 300 s.

Sample		7.5% in CELD bath	15% in CELD bath
Pr in film	XRF	10.5 ± 0.6	20.9 ± 1.2
[at%]	ICP-MS	11.5 ± 0.4	21.9 ± 0.8

band diagram is also shown in Figure S3 (Supporting Information).

Figure 2a shows the typical impedance spectra of symmetric cells with pristine and PCO-coated Pt electrodes obtained when $T = 500\text{ }^{\circ}\text{C}$ and $p\text{O}_2 = 0.21\text{ atm}$. While the offset resistance (R_{off}) at a higher frequency remains nearly identical for both electrodes, the arc in the lower frequency regime decreases remarkably after the PCO coating. R_{off} exhibits activation energy (E_a) of $\approx 1.1\text{ eV}$ and does not change with $p\text{O}_2$. Furthermore, the magnitude of the conductivity ($1.2 \times 10^{-3}\text{ S cm}^{-1}$ at $600\text{ }^{\circ}\text{C}$), calculated based on the cell geometry and measured value of R_{off} , is in good agreement with the literature value for the YSZ single-crystal material ($1.6 \times 10^{-3}\text{ S cm}^{-1}$ at $600\text{ }^{\circ}\text{C}$).^[24] Thus, R_{off} can be solely attributed to the YSZ electrolyte.

Accordingly, the remaining spectra at a lower frequency can be attributed to the electrode response, which is our main concern. The overcoated nanostructured PCO layers dramatically improve the electrode activity, as evidenced by the diameter of the semicircle, which decreases substantially. For example, the Pt electrode resistance of $\approx 170 \times 10^3\ \Omega$ at $500\text{ }^{\circ}\text{C}$ and $p\text{O}_2 = 0.21\text{ atm}$ is decreased by more than 1000 times to $\approx 120\ \Omega$ after the coating process. Significantly, only 5 min of PCO coating resulted in such a large decrease in the electrode resistance, confirming the important role of PCO for ORR.

We analyzed the specific features of the electrode impedances further, by examining the dependence of the temperature, $p\text{O}_2$, and electrode geometry. For bare Pt electrodes, a near-ideal arc was modeled by a R - Q circuit, where R is the resistance, Q is the constant-phase element (CPE), and the overall impedance is represented by

$$Z_Q = \frac{1}{Q(i\omega)^n} \quad (1)$$

The effective capacitance could be determined with using the equation

$$C = (R^{1-n}Q)^{1/n} \quad (2)$$

It was noted that the bare Pt electrodes show typical double-layer capacitance with a value of $\approx 10^{-4}\text{ F cm}^{-2}$,^[25] where the corresponding electrode resistance depends almost linearly on the 3PB site density, as shown in Figure S4 (Supporting Information). As is well known, such features undoubtedly reveal that the ORR reactions occur mainly at the 3PB sites in the Pt electrodes.

Next, turning to the PCO-coated Pt electrodes, a slightly distorted arc was observed, which was fitted with two serial R - Q circuit elements (inset in Figure 2a). Here, the R and C values derived from the arc at the higher frequency (blue line) and that at a lower frequency (red line) are denoted as R_{HF} and C_{HF} , and R_{LF} and C_{LF} , respectively. In this study, we briefly describe the physical causes of the two impedance arcs. For the impedance arc at a lower frequency, C_{LF} exhibits a relatively large value ranging from 0.319 to 0.673 mF cm^{-2} and $\approx -1/6$ slope dependence of $\log C_{\text{LF}}$ on $\log p\text{O}_2$ (Figure 2b),^[23,26] which is consistent with the concept of the chemical capacitance reported in the literature on mixed conducting oxide electrodes.^[27–29] The chemical capacitance originates from a

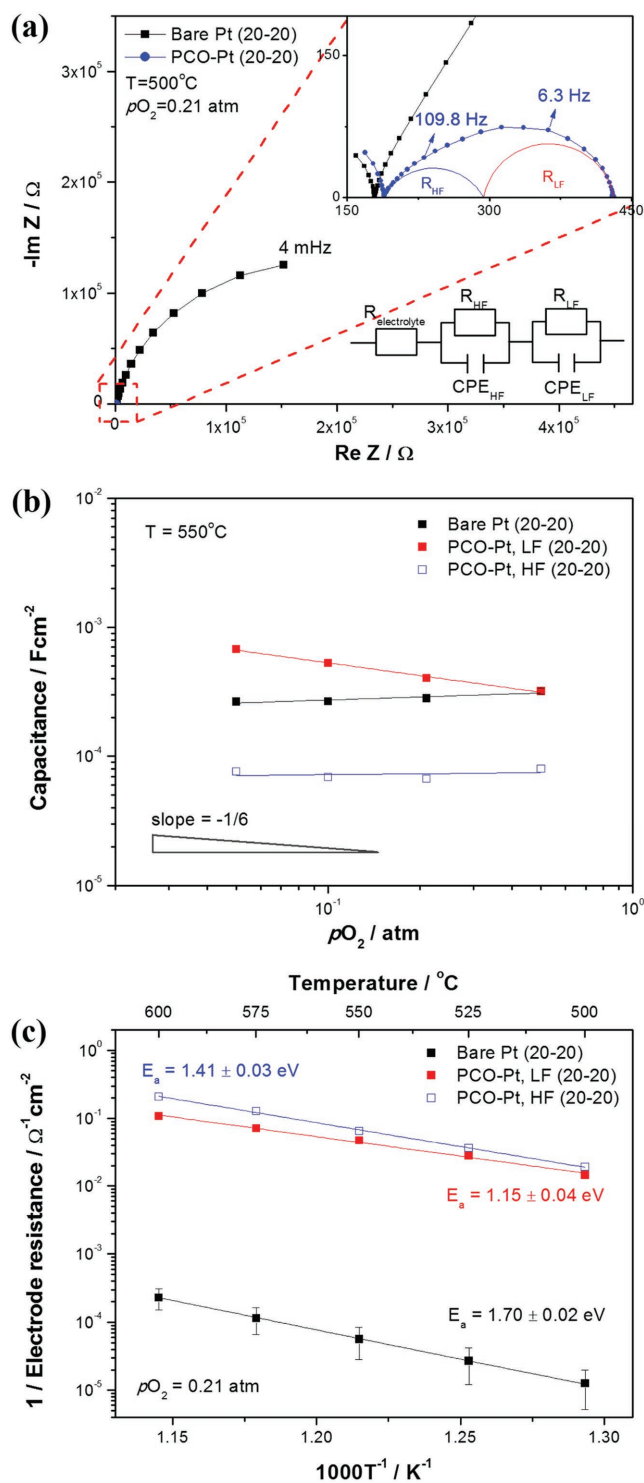


Figure 2. a) Typical impedance spectra of bare and (Pr,Ce) $\text{O}_{2-\delta}$ (PCO)-coated Pt electrodes on both sides of a yttria-stabilized ZrO_2 (YSZ) single-crystal electrolyte substrate with $T = 500\text{ }^{\circ}\text{C}$ and $p\text{O}_2 = 0.21\text{ atm}$. The magnified spectrum of PCO-coated Pt electrodes indicates two distinct arcs at a higher frequency (HF, blue) and a lower frequency (LF, red). b) Double-logarithmic plots of the capacitance versus $p\text{O}_2$ dependence of both electrodes when $T = 550\text{ }^{\circ}\text{C}$ and $p\text{O}_2 = 0.05\text{--}0.5\text{ atm}$. c) Temperature dependence of the electrode conductance of both electrodes when $T = 500\text{--}600\text{ }^{\circ}\text{C}$ and $p\text{O}_2 = 0.21\text{ atm}$.

capacitive process resulting from changes in the oxygen content in response to the applied electrical potential perturbation. In fact, the surface electrochemical reaction of mixed conducting oxide electrodes, specifically ORR, has been shown to occur frequently in parallel with this capacitance,^[26,30] suggesting that R_{LF} corresponds to the electrochemical reaction. On the other hand, the high-frequency response is attributed to constriction effects ensuing from the tortuous electron pathway from surface reaction sites to the embedded metal current collectors or the similarly tortuous ion pathway from the surface reaction sites to the YSZ electrolyte. Such effects are observed in related measurement configurations.^[20,31] This is supported further by the fact that C_{HF} is relatively small at 0.067–0.080 mF cm⁻² and is independent of pO_2 . Accordingly, henceforth, we focus on R_{LF} , which represents the electrochemical reaction on the PCO surface, and discuss the changes in the ORR activity, defined as 1/electrode resistance normalized to the projected electrode area, of the Pt electrodes before and after the coating process.

Similar to bare Pt electrodes, the ORR activity (i.e., R_{LF}) is linearly dependent on 3PB length with a power law exponent of -1.0 (Figure S4, Supporting Information). Considering that the PCO layer is preferentially coated not only on the Pt pattern but also on the YSZ electrolyte around the edge of the Pt, the 3PB dependence of the electrode resistance in PCO-coated Pt electrodes is natural. Nonetheless, the enhanced electrode activity indicates that the PCO layer itself is highly active for ORR. The temperature dependence of the ORR activity of the bare and PCO-coated Pt electrodes is shown in Figure 2c. The slope in an Arrhenius-type plot reflects the activation energy (E_a) associated with the ORR. The bare Pt electrode exhibits an E_a value of 1.70 eV, which is a typical characteristic of Pt electrodes at relatively low temperatures.^[32] On the other hand, the E_a value of the PCO-coated Pt electrodes is much smaller at 1.15 eV, similar to the reported value of 1.26 eV for a dense PCO thin-film electrode.^[30] The E_a value reduced by the coating implies that the ORR itself changes with the presence of PCO. Although atomic/molecular-level reaction mechanisms are outside the scope of this study, it is obvious that the ORR occurs on the PCO surface after the coating process.

To confirm our assertion, we fabricated electrodes with three different overcoat thicknesses by varying the CELD deposition times and compared the E_a values of the ORR activity and the pO_2 dependence of C_{LF} (Figure S5, Supporting Information). The electrode activity continues to increase with the CELD deposition time (Figure S5a, Supporting Information). Taking into account that the PCO thickness and thus surface area increases with the deposition time (Figure S6 and Table S1, Supporting Information), this result clearly shows again that 2PB sites are the main reaction sites of ORR on the PCO-coated Pt electrodes. More specifically, as the CELD deposition time increases, the magnitude of the ORR activity increases

and corresponding E_a value decreases steadily (Figure S5b,c, Supporting Information). Similarly, as the deposition time increases, the value of C_{LF} and the slope of $\log C_{LF}$ on $\log pO_2$ become closer to the characteristics ($C_{LF} \propto pO_2^{-1/6}$) predicted by the charge carrier concentrations of the bulk PCO at the given temperature and pO_2 (Figure S5d,e, Supporting Information). Therefore, as the thickness of the PCO overcoats increases, the characteristics of the PCO-coated Pt electrode change from that of Pt to that of the pristine PCO itself. This is also supported by the results of a distribution of relaxation times (DRT) analysis (Figure S7, Supporting Information),^[33] in which a shift of the intermediate characteristic frequency peaks according to pO_2 is observed, indicating that R_{LF} with a longer relaxation time is associated with the electrochemical reaction process on 2PB. Taking all of these observations into account, one can confidently conclude that ORR takes place actively on the PCO surface and that the PCO surface reaction becomes more dominant as the PCO thickness increases in the coated Pt thin-film electrodes.

In addition, the PCO-coated Pt films exhibit decent thermal stability (Figure 3a). The PCO overcoat itself is very stable at high temperatures, and the nanoscale architecture of the films does not collapse or become aggregated. As shown in Figure 3b,c, the PCO overcoat retains the high-surface-area structure of the as-deposited coat even after a 10 h heat treatment at 700 °C. Furthermore, the PCO layer partially suppresses the sintering of porous Pt thin films. It has been frequently reported in research on catalysis that the thermal stability of Pt can be improved by a ceria-based coating/supporting layer.^[34–37] Previously, we also demonstrated that the durability of Pt thin-film electrodes with nanoscale pores was sufficiently improved by a CELD coating of Sm-doped ceria.^[11] To confirm this, here we fabricated porous Pt thin films with a nanoscale pore size and a thickness of only several tens of nanometers, as commonly used in TF-SOFCs, and measured how the sheet resistance of the thin films after a heat treatment varied with the presence

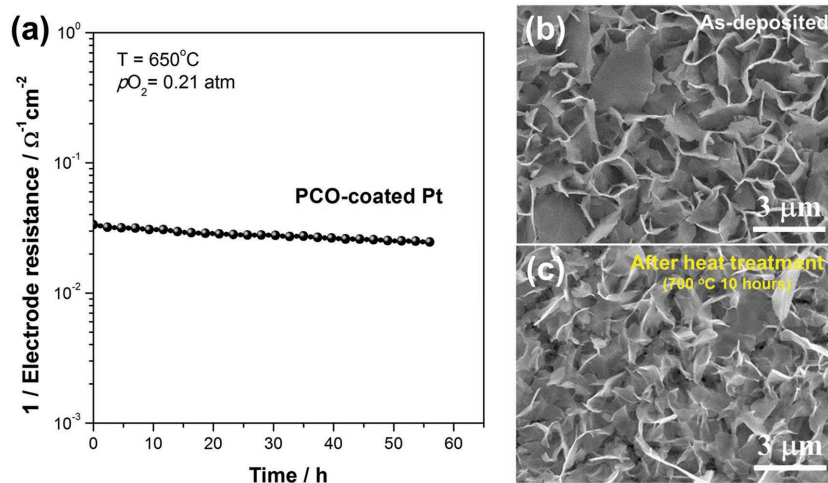


Figure 3. a) High-temperature stability of (Pr,Ce)O_{2-δ} (PCO)-coated Pt electrodes for an oxygen reduction reaction (ORR) when $T = 650$ °C and $pO_2 = 0.21$ atm. SEM images of b) an as-deposited and c) a heat-treated PCO layer. The heat treatment was carried out at 700 °C for 10 h. Cathodic electrochemical deposition (CELD) was conducted at -0.8 V versus saturated calomel electrode (SCE) for a deposition time of 300 s.

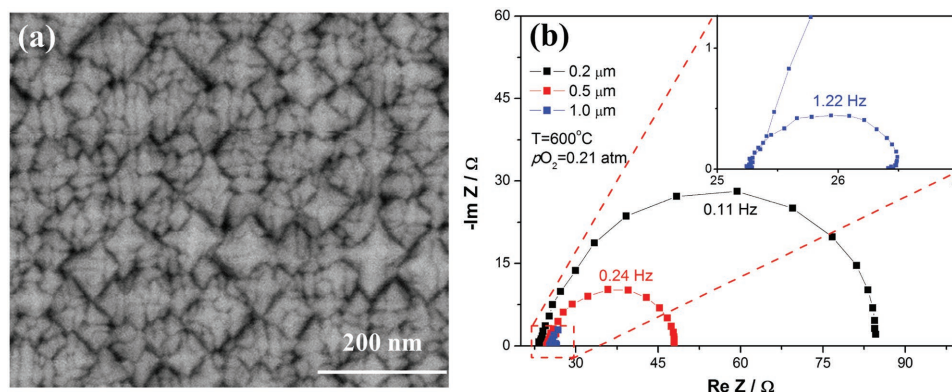


Figure 4. a) SEM image and b) impedance spectra of nano-columnar $(\text{Pr,Ce})\text{O}_{2-\delta}$ (PCO) structures prepared under 120 mTorr O_2 at 600 °C.

of the PCO overcoat. As shown in Figure S8 (Supporting Information), after the 24 h heat treatment at 650 °C, the porous Pt film coarsens and the connectivity becomes seriously degraded. As a result, the sheet resistance at room temperature is greatly increased, so that it cannot be measured. In contrast, PCO-coated Pt thin films show little change in sheet resistance after the heat treatment. These observations support the contention that the PCO CELD coating appears to protect the Pt electrode to some extent from sintering.

Because PCO itself has been shown to function very well as an electrode, we were able to design a new electrode architecture consisting of only PCO without Pt. Here, the key to the electrode design is to maximize the specific surface area of PCO, the main ORR reaction sites. To test this idea, we fabricated highly porous, vertically oriented columnar PCO thin films with extremely high 2PB densities via pulsed laser deposition (PLD), as shown in Figure 4a. It was found that even without an optimization step, an electrode resistance value of $0.6 \Omega \text{ cm}^2$ at 600 °C could be achieved with a film thickness of merely 1 μm (Figure 4b). The electrode performance of the nano-columnar PCO is even comparable to the world-record value of the state-of-the-art perovskite oxide of $\text{La}_{0.6}\text{Sr}_{0.4}\text{O}_{3-\delta}$ ($0.8 \Omega \text{ cm}^2$, 5- μm -thick film)^[38] when the comparison group is limited to electrodes made with a thin-film process applicable to TF-SOFCs (Figure 5).^[38–45]

In conclusion, we successfully fabricated PCO-Pt composite films as a model system to evaluate the impact of PCO overcoats quantitatively on the activity and stability of Pt thin-film O_2 -electrode at temperatures between 500 and 600 °C. Nanostructured PCO is uniformly grown on a Pt surface via a simple and cost-effective CELD method. The PCO coating dramatically enhances the electrode activity by more than 1000 times due to the predominant reaction sites expanding from 3PB (Pt|YSZ| O_2) to 2PB (PCO| O_2). Furthermore, the PCO-coated Pt films exhibit decent thermal stability for 60 h at a relatively high temperature of 650 °C. Based on these observations, for the first time, we designed and fabricated metal-free, nano-columnar PCO films with an enhanced 2PB area and succeeded in achieving exceptional electrode performances with resistance of $0.6 \Omega \text{ cm}^2$ at 600 °C. In summary, these findings provide useful guidance for the design and fabrication of high-performance TF-SOFC cathodes.

Experimental Section

Preparation of Model Electrochemical Cells with Pt Patterned Films: Model electrochemical cells with Pt patterned electrodes were deposited on both sides of (100) single-crystal YSZ (8 mol%, 10 mm × 10 mm × 0.5 mm, MTI Corp.) substrates serving as the oxygen-ion-conducting electrolyte. Pt patterns were fabricated by a photolithographic lift-off process. First, a positive photoresist (AZ5214) was spin-coated onto the YSZ substrate at 3000 rpm for 30 s, and baked at 115 °C for 60 s. Next, the mask plate with defined chromium patterns was aligned with the samples in a contact aligner and exposed to ultraviolet light for 10–12 s. The samples were then immersed AZ 300 MIF solution to develop the photoresist. After rinsing by deionized water and drying, the photoresist was baked at 120 °C for 120 s. Pt thin films with a thickness of $\approx 200 \text{ nm}$ were sputtered by DC magnetron sputtering at a DC power of 100 W in an Ar working pressure of 5 mTorr. Metal lift-off was achieved by immersing the samples in acetone at room temperature. The patterned samples were first annealed at 800 °C for 2 h to avoid microstructural

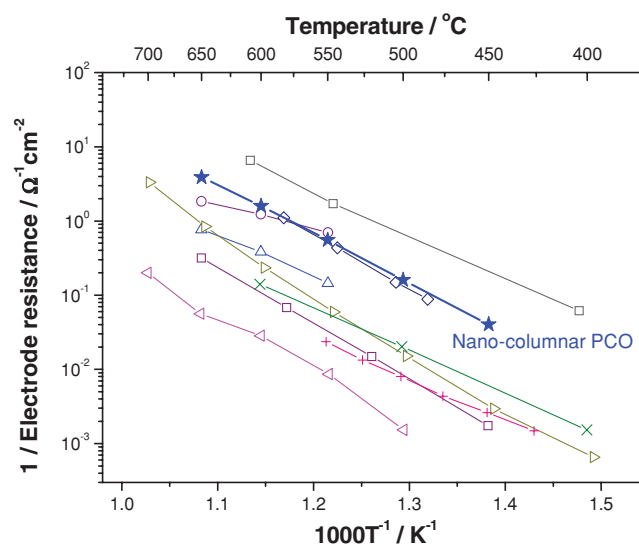


Figure 5. Arrhenius plot of the electrode activities of 1- μm -thick nano-columnar $(\text{Pr,Ce})\text{O}_{2-\delta}$ (PCO) films created via pulsed laser deposition (PLD) in this study. The reported electrode activities of other perovskite oxides are inserted for comparison. PLD: (○) = $\text{La}_{0.6}\text{Sr}_{0.4}\text{CoO}_3$,^[38] (Δ) = $\text{La}_{0.8}\text{Sr}_{0.2}\text{CoO}_3$,^[38] (□) = $\text{La}_{0.6}\text{Sr}_{0.4}\text{Co}_{0.2}\text{Fe}_{0.8}\text{O}_3$,^[39] (◻) = $\text{La}_{0.4}\text{Sr}_{0.6}\text{Co}_{0.8}\text{Fe}_{0.2}\text{O}_3$,^[40] (◊) = $\text{La}_{0.6}\text{Ca}_{0.4}\text{Fe}_{0.8}\text{Ni}_{0.2}\text{O}_3$,^[41] (◁) = $\text{La}_{0.6}\text{Sr}_{0.4}\text{CoO}_3$,^[42] (◇) = $\text{La}_{0.6}\text{Sr}_{0.4}\text{CoO}_3$,^[43] RF sputtered: (+) = $\text{La}_{0.6}\text{Sr}_{0.4}\text{Co}_{0.8}\text{Fe}_{0.2}\text{O}_3$,^[44] (×) = $\text{La}_{0.6}\text{Sr}_{0.4}\text{CoO}_3$.^[45]

evolution during electrochemical measurements. Electrochemical measurements were performed using Pt strip widths of 10, 20, 40, and 80 μm , corresponding to 3PB densities ranging from 85 to 645 cm^{-2} .

Electrochemical Deposition of PCO Films: An aqueous electrolyte solution was prepared with nitrate-based cation precursors, $\text{Ce}(\text{NO}_3)_3 \cdot 6\text{H}_2\text{O}$ (99.99%, Alfa Aesar) and $\text{Pr}(\text{NO}_3)_3 \cdot 6\text{H}_2\text{O}$ (99.9%, Sigma-Aldrich). Total cation molar concentration was fixed at 0.05 M and CELD was performed by varying the concentration of Pr^{3+} in the solution bath to 7.5 and 15%. A traditional three-electrode system was used with a reference electrode (SCE, +0.24 V vs standard hydrogen electrode (SHE), Koslow), and a counter electrode (carbon rod). Electrical contact with the Pt patterned films, deposited on both sides of the YSZ substrates, was accomplished using tailor-made aluminum clip, which served as a working electrode. Electrochemical deposition was performed at room temperature and ambient atmosphere in the potentiostat mode. A fixed electric potential of -0.8 V (vs SCE) between the working electrode and the reference electrode was applied and the resulting current from the counter electrode to the working electrode was measured. The CELD deposition time varied from 60 to 300 s.

Preparation of Electrochemical Cells with Nano-columnar PCO Films: A nano-columnar $\text{Pr}_{0.2}\text{Ce}_{0.8}\text{O}_{2-\delta}$ film was grown via PLD from oxide targets of the respective materials. The PLD targets were prepared by a combined EDTA-citrate complexing method, starting from $\text{Ce}(\text{NO}_3)_3 \cdot 6\text{H}_2\text{O}$ and $\text{Pr}(\text{NO}_3)_3 \cdot 6\text{H}_2\text{O}$ precursors. The precursors were dissolved into deionized water with chelating agents (EDTA and citric acid), and NH_4OH was added to adjust the pH to 9.5. The resulting mixture was kept at 80 $^\circ\text{C}$ until a gel formed. After drying, the gel was fired at 450 $^\circ\text{C}$ for 3 h to obtain PCO powder. The subsequent calcination was conducted at 750 $^\circ\text{C}$ for 6 h in air and the resulting powder was isostatically cold-pressed at 200 MPa. The compacted green body was sintered at 1400 $^\circ\text{C}$ for 6 h. Symmetric cells with a nano-columnar PCO electrode were prepared on both sides of YSZ substrates by PLD, operated with a KrF excimer laser, emitting at 248 nm (Coherent COMPex Pro 205), at energy of 235 mJ pulse $^{-1}$ with a repetition rate 20 Hz. The deposition temperature and atmosphere were 600 $^\circ\text{C}$ and 120 mTorr O_2 , respectively. A thickness of PCO films was varied between 0.2 and 1.0 μm by varying deposition time from 8 to 30 min.

Material Characterizations: Film microstructures were examined by SEM (Hitachi S-4800). An ICP-MS (Agilent ICP-MS 7700S) analysis and XRF (Rigaku ZSX Primus II) measurement were undertaken to measure the chemical composition of the coated PCO layers precisely. The surface area of the coated PCO films was obtained by Brunauer-Emmett-Teller (BET) measurements (Autosorb-iQ 2ST/MP (Quantachrom Corp.), Kr at 77.3 K).

Electrochemical Measurements: Electrochemical analyses of symmetric cells with bare and PCO-coated Pt electrodes were carried out by AC impedance spectroscopy (ACIS, VSP-300, Biologic). The cells were located inside a continuous-flow alumina tube for ACIS test into which mixtures of O_2 and Ar were delivered through digital mass flow controllers. Impedance spectra were obtained at temperatures between 500 and 600 $^\circ\text{C}$ and at an oxygen partial pressure between 0.05 and 0.5 atm with AC amplitude of 20 mV at a frequency range of 2 MHz to 4 mHz. The long-term stability of PCO-coated Pt electrodes was then evaluated for 60 h at 650 $^\circ\text{C}$ with 0.21 atm O_2 . In case of nano-columnar PCO symmetric cells, impedance measurements were performed at temperatures ranging from 450 to 650 $^\circ\text{C}$ and other conditions were the same as above.

Supporting Information

Supporting Information is available from the Wiley Online Library or from the author.

Acknowledgements

This work was supported by the Korea Institute of Energy Technology Evaluation and Planning (KETEP) and the Ministry of Trade, Industry &

Energy (MOTIE) of the Republic of Korea (No. 20163030031850). Additional support was provided by the Korea Electric Power Corporation (KEPCO) Research Institute.

Conflict of Interest

The authors declare no conflict of interest.

Keywords

cathodic electrochemical deposition, oxygen reduction reaction, $(\text{Pr,Ce})\text{O}_{2-\delta}$, thin-film solid oxide fuel cells

Received: December 27, 2017

Revised: February 8, 2018

Published online: March 13, 2018

- [1] E. D. Wachsman, K. T. Lee, *Science* **2011**, 334, 935.
- [2] H. L. Tuller, S. J. Litzelman, W. Jung, *Phys. Chem. Chem. Phys.* **2009**, 11, 3023.
- [3] Z. Shao, S. M. Haile, *Nature* **2004**, 431, 170.
- [4] A. Evans, A. Bieberle-Hutter, J. L. M. Rupp, L. J. Gauckler, *J. Power Sources* **2009**, 194, 119.
- [5] J. An, J. H. Shim, Y. B. Kim, J. S. Park, W. Lee, T. M. Gur, F. B. Prinz, *MRS Bull.* **2014**, 39, 798.
- [6] D. Beckel, A. Bieberle-Hutter, A. Harvey, A. Infortuna, U. P. Muecke, M. Prestat, J. L. M. Rupp, L. J. Gauckler, *J. Power Sources* **2007**, 173, 325.
- [7] C. W. Kwon, J. W. Son, J. H. Lee, H. M. Kim, H. W. Lee, K. B. Kim, *Adv. Funct. Mater.* **2011**, 21, 1154.
- [8] M. Tsuchiya, B. K. Lai, S. Ramanathan, *Nat. Nanotechnol.* **2011**, 6, 282.
- [9] S. B. Adler, *Chem. Rev.* **2004**, 104, 4791.
- [10] N. P. Brandon, S. Skinner, B. C. H. Steele, *Annu. Rev. Mater. Res.* **2003**, 33, 183.
- [11] H. G. Seo, Y. Choi, B. Koo, A. Jang, W. Jung, *J. Mater. Chem. A* **2016**, 4, 9394.
- [12] W. Jung, J. J. Kim, H. L. Tuller, *J. Power Sources* **2015**, 275, 860.
- [13] C. C. Yu, S. Kim, J. D. Baek, Y. Li, P. C. Su, T. S. Kim, *ACS Appl. Mater. Interfaces* **2015**, 7, 6036.
- [14] I. Chang, S. Ji, J. Park, M. H. Lee, S. W. Cha, *Adv. Energy Mater.* **2015**, 5, 1402251.
- [15] S. R. Bishop, T. S. Stefanik, H. L. Tuller, *J. Mater. Res.* **2012**, 27, 2009.
- [16] H. L. Tuller, S. R. Bishop, D. Chen, Y. Kuru, J. J. Kim, T. S. Stefanik, *Solid State Ionics* **2012**, 225, 194.
- [17] S. R. Bishop, T. S. Stefanik, H. L. Tuller, *Phys. Chem. Chem. Phys.* **2011**, 13, 10165.
- [18] I. Zhitomirsky, A. Petric, *Ceram. Int.* **2001**, 27, 149.
- [19] E. C. Brown, *Ph.D. Thesis*, California Institute of Technology **2011**.
- [20] Y. Choi, E. C. Brown, S. M. Haile, W. Jung, *Nano Energy* **2016**, 23, 161.
- [21] D. R. Lide, *CRC Handbook of Chemistry and Physics*, 84th ed., CRC Press, Boca Raton, FL, USA **2003**.
- [22] K. Kamada, N. Enomoto, J. Hojo, *Electrochim. Acta* **2009**, 54, 6996.
- [23] D. Chen, *Ph.D. Thesis*, Massachusetts Institute of Technology **2014**.
- [24] W. D. Shen, J. L. Hertz, *J. Mater. Chem. A* **2015**, 3, 2378.
- [25] N. L. Robertson, J. N. Michaels, *J. Electrochem. Soc.* **1991**, 138, 1494.
- [26] D. Chen, H. L. Tuller, *Adv. Funct. Mater.* **2014**, 24, 7638.
- [27] W. Jung, H. L. Tuller, *Adv. Energy Mater.* **2011**, 1, 1184.

- [28] F. S. Baumann, J. Fleig, G. Cristiani, B. Stuhlhofer, H. U. Habermeier, J. Maier, *J. Electrochem. Soc.* **2007**, *154*, B931.
- [29] W. Jung, J. O. Dereux, W. C. Chueh, Y. Hao, S. M. Haile, *Energy Environ. Sci.* **2012**, *5*, 8682.
- [30] D. Chen, S. R. Bishop, H. L. Tuller, *J. Electroceram.* **2012**, *28*, 62.
- [31] W. Jung, K. L. Gu, Y. Choi, S. M. Haile, *Energy Environ. Sci.* **2014**, *7*, 1685.
- [32] A. K. Opitz, A. Lutz, M. Kubicek, F. Kubel, H. Hutter, J. Fleig, *Electrochim. Acta* **2011**, *56*, 9727.
- [33] T. H. Wan, M. Saccoccio, C. Chen, F. Ciucci, *Electrochim. Acta* **2015**, *184*, 483.
- [34] X. Wang, D. Liu, S. Song, H. Zhang, *J. Am. Chem. Soc.* **2013**, *135*, 15864.
- [35] S. Lee, J. Seo, W. Jung, *Nanoscale* **2016**, *8*, 10219.
- [36] H. Shinjoh, *Catal. Surv. Asia* **2009**, *13*, 184.
- [37] Y. Nagai, T. Hirabayashi, K. Dohmae, N. Takagi, T. Minami, H. Shinjoh, S. Matsumoto, *J. Catal.* **2006**, *242*, 103.
- [38] J. Hwang, H. Lee, K. J. Yoon, H. W. Lee, B. K. Kim, J. H. Lee, J. W. Son, *J. Electrochem. Soc.* **2012**, *159*, F639.
- [39] D. Beckel, U. P. Muecke, T. Gyger, G. Florey, A. Infortuna, L. J. Gauckler, *Solid State Ionics* **2007**, *178*, 407.
- [40] J. Yoon, R. Araujo, N. Grunbaum, L. Baque, A. Serquis, A. Caneiro, X. H. Zhang, H. Y. Wang, *Appl. Surf. Sci.* **2007**, *254*, 266.
- [41] I. R. de Larramendi, N. Ortiz, R. Lopez-Anton, J. I. R. de Larramendi, T. Rojo, *J. Power Sources* **2007**, *171*, 747.
- [42] I. Garbayo, V. Esposito, S. Sanna, A. Morata, D. Pla, L. Fonseca, N. Sabaté, A. Tarancón, *J. Power Sources* **2014**, *248*, 1042.
- [43] J. Januschewsky, M. Ahrens, A. Opitz, F. Kubel, J. Fleig, *Adv. Funct. Mater.* **2009**, *19*, 3151.
- [44] H. Xiong, B. K. Lai, A. C. Johnson, S. Ramanathan, *J. Power Sources* **2009**, *193*, 589.
- [45] A. Takeshita, S. Miyoshi, S. Yamaguchi, T. Kudo, Y. Sato, *Solid State Ionics* **2014**, *262*, 378.